metals

Article

Phase Equilibria in the Ni-V-Ta Ternary System

Cuiping Wang [1,*], Yuhui Liang [1], Shuiyuan Yang [1], Jinbin Zhang [1], Yixiong Huang [1], Jiajia Han [1], Yong Lu [1] and Xingjun Liu [1,2,*]

1 College of Materials and Fujian Key Laboratory of Materials Genome, Xiamen University, Xiamen 361005, China; 20720161150072@stu.xmu.edu.cn (Y.L.); yangshuiyuan@xmu.edu.cn (S.Y.); jbzhang@xmu.edu.cn (J.Z.); hyx@xmu.edu.cn (Y.H.); jiajiahan@xmu.edu.cn (J.H.); luyong@xmu.edu.cn (Y.L.)

2 State Key Laboratory of Advanced Welding and Joining, Harbin Institute of Technology, Shenzhen 518005, China

* Correspondence: wangcp@xmu.edu.cn (C.W.); lxj@xmu.edu.cn (X.L.); Tel.: +86-592-218-7888 (C.W.); Fax: +86-592-218-7966 (C.W.)

Received: 2 September 2018; Accepted: 25 September 2018; Published: 28 September 2018

Abstract: Two isothermal sections of the Ni-V-Ta ternary system at 1200 °C and 1000 °C have been experimentally established using X-ray diffraction, electron probe microanalysis, energy dispersive spectroscopy, and differential scanning calorimeter with equilibrated key alloys. The equilibrium composition of each phase is measured by electron probe microanalysis and energy dispersive spectroscopy. The results indicate that: (1) nine three-phase and eight three-phase regions were confirmed in the isothermal section at 1200 °C and 1000 °C, respectively; (2) the C14 phase with a large solubility of about 51.2 at. % Ni was observed at 1200 °C, while it forms a single-phase region at 1000 °C; (3) a small liquid region was confirmed at 1200 °C, but disappeared at 1000 °C.

Keywords: Ni-V-Ta system; phase equilibrium; liquid section; electron probe microanalysis

1. Introduction

Nickel-based superalloys have become unique materials used in gas turbine engines, due to their excellent mechanical properties, oxidation, and creep resistance at elevated temperatures [1]. With increasing industry requirements for better high-temperature strength materials, there is an urgent need to improve the high-temperature properties of these superalloys. Many studies have been carried out to confirm the fact that a small addition of refractory elements (e.g., Re, Ru and Ta) can improve the high-temperature strength [1–3]. Besides, in 1981, Yang [4] found that a trace addition of 1 at. % Ta in complex nickel-based alloys improved the oxidation resistance significantly. Recently, Park et al. [5] have found that Ta exerted a beneficial effect on oxidation resistance in nickel-based superalloys. Additionally, the Ni_3V ($D0_{22}$) phase is a critical phase in the dual two-phase intermetallic alloys composed of Ni_3Al and Ni_3V, which possessed outstanding mechanical and chemical properties [6–8]. However, there is limited information on the Ni-V-Ta ternary system [9,10]. In 1971, Moreen et al. [9] investigated the ordering reactions of Ni_8X (X: V, Ta, Nb) by electrical resistivity and electron diffraction techniques. Then, Gupta [10] reviewed the experimental data of the ternary system. Unfortunately, no information of experimental phase diagram and thermodynamic database was found for this ternary system. Therefore, it is essential to establish the phase relation of Ni-V-Ta ternary system for developing thermodynamic database and practical application.

The Ni-V-Ta ternary system consists of three sub-systems: Ni-Ta, Ni-V, and V-Ta binary system, as shown in Figure 1. All the stable compounds and solid solutions are summarized in Table 1.

The Ni-Ta system was systematically investigated by several researchers [11–23]. Solid solution face-centered cubic (fcc), body-centered cubic (bcc-(Ta)), and five intermetallic compounds (Ni_8Ta, Ni_3Ta, Ni_2Ta, Ni_6Ta_7 and6 $NiTa_2$) coexist in this binary system according to Nash et al. [16] and

Pan et al. [20]. There are three peritectic reactions and two eutectic reactions in the binary system. The $NiTa_2$ and Ni_6Ta_7 phases form from the peritectic reaction L + bcc-(Ta) ↔ $NiTa_2$ at 1788 °C and L + $NiTa_2$ ↔ Ni_6Ta_7 at 1570 °C, respectively. At 1330 °C, the eutectic reaction L ↔ Ni_3Ta + fcc occur. Meanwhile, the thermodynamic information of this binary system was assessed by several investigators [16–22] with the Computer Coupling of Phase Diagrams and Thermochemistry (CALPHAD) approach and first-principles calculation. The Ni-Ta phase diagram adopted in present work was assessed by Nash et al. for its better agreement with the experimental results.

The Ni-V phase diagram was well studied by many investigators [24–27]. There are two terminal solid solutions (fcc, bcc-(V)) and five intermetallic compounds (σ′, Ni_8V, Ni_3V, Ni_2V and NiV_3) in this system according to Smith et al. [24]. Two eutectoids, a eutectic, a peritectic, a peritectoid, and three congruent transformations exist in the system. The Ni_3V phase forms from a congruent transformation at 1045 °C. The information of the Ni-V system was thermodynamically analyzed by Watson et al. [26] and Kabanova et al. [27], which were in agreement with the experimental results.

As for the V-Ta binary system, a continuous solid solution bcc-(V, Ta) at elevated temperatures and an intermediate phase (V_2Ta) at lower temperatures were identified according to the previous work [28–32]. However, the focus lay on the phase transition of Laves phase at low temperatures. In 1972, Savieky et al. [28] confirmed a C15-type ($MgCu_2$) phase and C14-type ($MgZn_2$) phase two-phase field at the temperature range of 1125 °C to 1280 °C. Later, Danon et al. [30] and Pavlů et al. [32] evaluated the V-Ta system by CALPHAD approach and first-principles calculation.

Thus, because of the lacking information of the Ni-V-Ta system, the goal of this work was to establish the isothermal sections of the Ni-V-Ta ternary system at 1000 °C and 1200 °C.

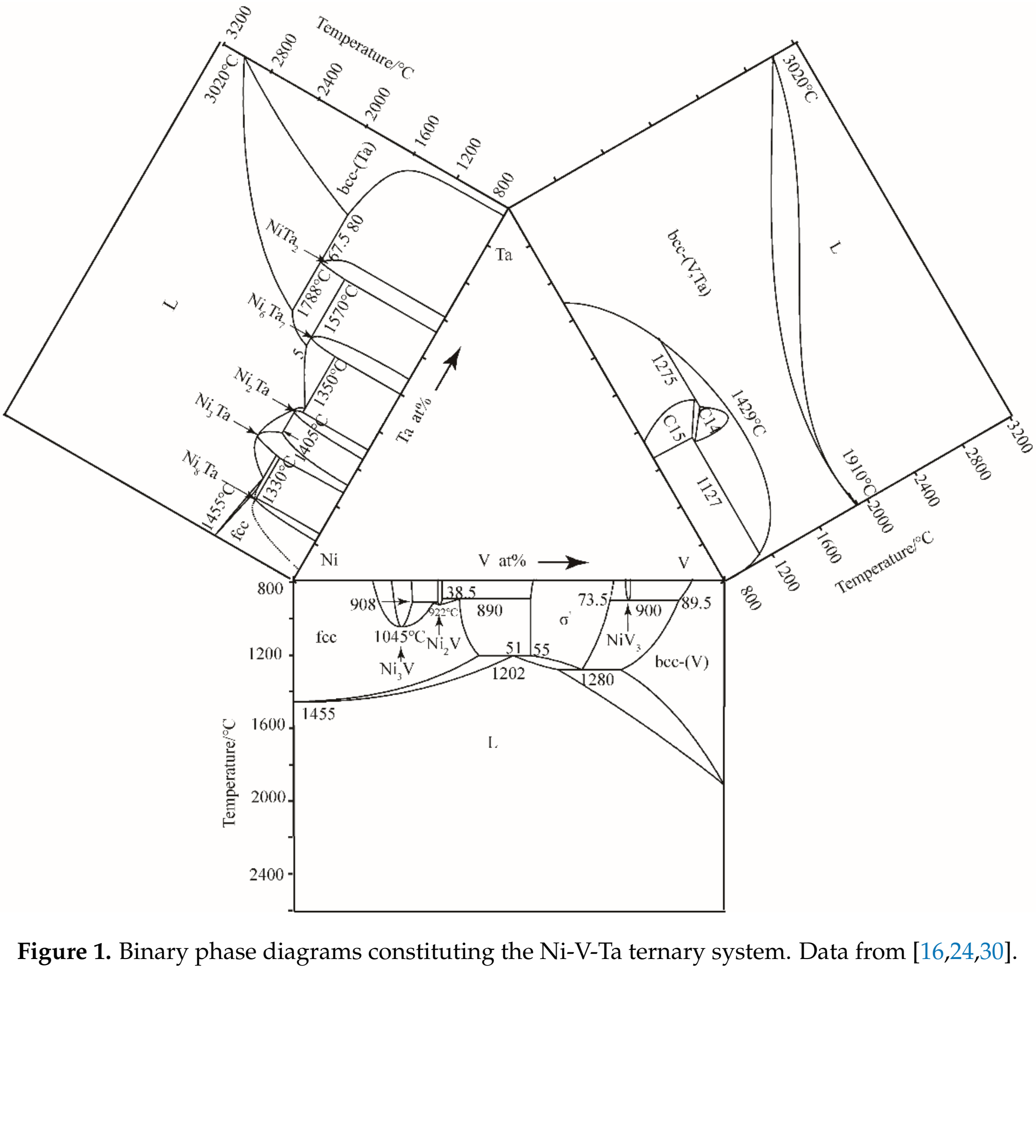

Figure 1. Binary phase diagrams constituting the Ni-V-Ta ternary system. Data from [16,24,30].

Table 1. The stable solid phases in the three binary systems. Data from [16,24,30].

System	Phase	Pearson Symbol	Prototye	Space Group	Strukturbericht	References
Ni-Ta	fcc	*cF4*	Cu	*Fm-3m*	A1	[16]
	Ni_8Ta	*tI36*	Ni_8Nb	*I4/mmm*		[16]
	Ni_3Ta	*tI8*	$TiAl_3$	*I4/mmm*	$D0_{22}$	[16]
		mP16	$NbPt_3$	$P2_1/m$		[16]
		oP8	Cu_3Ti	*Pmmn*	$D0_a$	[16]
	Ni_2Ta	*tI6*	$MoSi_2$	*I4/mmm*	$C11_b$	[16]
	Ni_6Ta_7	*hR39*	Fe_7W_6	*R-3mh*	$D8_5$	[16]
	$NiTa_2$	*tI12*	Al_2Cu	*I4/mcm*	C16	[16]
	bcc-(Ta)	*cI2*	W	*Im-3m*	A2	[16]
Ni-V	fcc	*cF4*	Cu	*Fm-3m*	A1	[24]
	Ni_8V	*tI18*	Ni_8Nb	*I4/mmm*		[24]
	Ni_2V	*oI6*	$MoPt_2$	*Immm*		[24]
	Ni_3V	*tI8*	Al_3Ti	*I4/mmm*	$D0_{22}$	[24]
	σ'	*tP30*	σ	$P4_2/mnm$		[24]
	NiV_3	*cP8*	Cr_3Si	*Pm3n*		[24]
	bcc-(V)	*cI2*	W	*Im-3m*	A2	[24]
V-Ta	bcc-(V, Ta)	*cI2*	W	*Im-3m*	A2	[30]
	C14	*hP12*	$MgZn_2$	$P6_3/mmc$	C14	[30]
	C15	*cF4*	$MgCu_2$	*Fd-3m*	C15	[30]

2. Experimental Details

The raw materials were the following high purity metals: nickel (99.9 wt. %), vanadium (99.9 wt. %) and tantalum (99.9 wt. %). All alloys were prepared in the form of atomic ratios (at. %). Bulk alloys with nominal composition were prepared by arc furnace melting in a high purity argon atmosphere with a non-consumable tungsten electrode on a water-cooled copper platform. The ingots, about 20 g, were re-melted at least five times to obtain homogeneous alloys with less than 0.5 wt. % weight loss.

All plate-shaped specimens were individually sealed in silica capsules backfilled with high purity argon, and annealed at 1000 °C for 55 days and 1200 °C for 40 days, respectively. Moreover, pure yttrium fillings were filled into the quartz capsules to prevent oxidation, and the alloys with liquid phase were wrapped in the pure tantalum slice to prevent contact reaction with quartz.

After heat treatment and metallographic preparation, the equilibrium compositions of all phases in specimens were determined by electron probe microanalysis (EPMA) with 20 kV accelerating voltage and 1.0×10^{-8} A probe current. The measured values were calibrated by ZAF (Z: atomic number effect, A: absorption effect, F: fluorescence effect) correction, with pure elements were used as standard samples. Energy-dispersive spectrometry (EDS) was used to measure the alloys' nominal composition and liquid phase composition. In order to identify the crystal structure, we used powder X-ray diffraction (XRD), with a Phillips Panalytical X-pet diffractometer using Cu-Kα radiation at 40 kV and 40 mA. The data were collected in the range of 2θ from 20 to 90 °C with a step interval of 0.015308° and a count time of 0.4 s per step. The melting points of the alloys were determined by differential scanning calorimeter (DSC) with a heating and cooling rate of 10 °C/min.

3. Results and Discussion

3.1. Phase Equilibria at 1000 °C

For the construction of isothermal section of the Ni-V-Ta ternary system at 1000 °C, 38 alloys were prepared and the equilibrium composition of each phase was summarized in Table 2.

Table 2. Equilibrium compositions of the phase in the Ni-V-Ta ternary alloys annealed at 1000 °C for 55 days.

Nominal Alloys (at. %)	**Phase Equilibrium**	**Composition (at. %)**					
	Phase 1/Phase 2/Phase 3	Phase 1		Phase 2		Phase 3	
		V	**Ta**	**V**	**Ta**	**V**	**Ta**
$Ni_{24}V_{67}Ta_9$	bcc-(V)/σ′/C14	90	3.1	70.6	5.2	47.1	27.1
$Ni_{13}V_{65}Ta_{22}$	bcc-(V)/C14	90.5	5.3	49.8	30.1		
$Ni_{41}V_{49}Ta_{10}$	σ′/C14	54.2	4.4	31.8	21.8		
$Ni_9V_{41}Ta_{50}$	bcc-(Ta)/C14	37	58.5	47.3	36.2		
$Ni_{61}V_{30}Ta_9$	fcc/Ni_3Ta/σ′	36.4	3.2	13.2	15	51.6	2.7
$Ni_{59}V_{24}Ta_{17}$	σ′/C14/Ni_3Ta	53	4.7	31	22.1	6.8	19.8
$Ni_{48}V_{18}Ta_{34}$	Ni_6Ta_7/C14/Ni_3Ta	17.9	47	23.5	29	2.5	24.1
$Ni_{77}V_{14}Ta_9$	fcc/Ni_3V/Ni_3Ta	13.1	4.6	17	6.7	12	12.4
$Ni_{19}V_{11}Ta_{70}$	bcc-(Ta)/Ni_6Ta_7/$NiTa_2$	9.6	88.3	14.5	51.5	2.2	65.9
$Ni_{17}V_{61}Ta_{22}$	bcc-(V)/C14	90.3	4.8	46.5	29.5		
$Ni_{52}V_{45}Ta_3$	fcc/σ′	37.9	2.8	51.8	2.7		
$Ni_{26}V_{34}Ta_{40}$	Ni_6Ta_7/C14	26.1	45	37.3	37.9		
$Ni_{68}V_{15}Ta_{17}$	Ni_3Ta/σ′	8.1	18.6	52.5	3.8		
$Ni_{64}V_5Ta_{31}$	Ni_2Ta/Ni_3Ta/Ni_6Ta_7	3.4	30.6	1.1	25.2	15.8	47.5
$Ni_{82}V_7Ta_{11}$	Ni_8Ta/Ni_3Ta	8.9	7.1	6.5	17		
$Ni_{18}V_{23}Ta_{59}$	Ni_6Ta_7/bcc-(Ta)	23.1	49	22	74.9		
$Ni_8V_{28}Ta_{64}$	Ni_6Ta_7/bcc-(Ta)	30	46.9	26.6	70		
$Ni_5V_{49}Ta_{46}$	C15/bcc-(Ta)	55.5	35.3	41.1	56.3		
$Ni_6V_{71}Ta_{23}$	C15/bcc-(V)	58.4	30.5	90.7	7.5		
$Ni_{35}V_{50}Ta_{15}$	σ′/C14	62.5	5.9	37.5	25		
$Ni_{71}V_{19}Ta_{10}$	fcc/Ni_3Ta	33.7	2.5	17.1	11		
$Ni_{79}V_{10}Ta_{11}$	fcc/Ni_3Ta	12.2	5.3	10.2	14.3		
$Ni_{50}V_6Ta_{44}$	Ni_2Ta/Ni_6Ta_7	2.1	34	6.7	48.8		
$Ni_{39}V_4Ta_{57}$	$NiTa_2$/Ni_6Ta_7	0.6	64.1	6.5	52.9		
$Ni_9V_2Ta_{89}$	$NiTa_2$/bcc-(Ta)	1	69.1	3.1	94.5		
$Ni_7V_{13}Ta_{80}$	Ni_6Ta_7/bcc-(Ta)	18	50.2	15.1	81.9		
$Ni_{59}V_{17}Ta_{24}$	Ni_3Ta/C14	3.5	22.6	25.2	26.4		
$Ni_{37}V_{35}Ta_{28}$	C14	35	28				
$Ni_{34}V_{33}Ta_{33}$	C14	33	33				
$Ni_{44}V_{26}Ta_{30}$	C14	26	30				
$Ni_4V_{68}Ta_{28}$	C15/bcc-(V)	61.2	31.5	90.1	8.5		
$Ni_5V_{54}Ta_{41}$	C15/bcc-(Ta)	56.5	37	39.8	48.9		
$Ni_{13}V_{46}Ta_{41}$	bcc-(Ta)/C14	39.1	57.8	51	35		
$Ni_{14}V_{36}Ta_{50}$	Ni_6Ta_7/C14/bcc-(Ta)	31.6	45.2	44.1	36.4	28.7	66.4
$Ni_{18}V_{55}Ta_{27}$	C14/bcc-(V)	50.2	31	90.2	5.4		
$Ni_{81}V_1Ta_{18}$	Ni_8Ta/Ni_3Ta	1.5	11.5	0.7	22.5		
$Ni_{12}V_{62}Ta_{26}$	C14/bcc-(V)	52	31.3	91.3	4.8		
$Ni_{33}V_{25}Ta_{42}$	Ni_6Ta_7/C14	21.4	45.9	29.8	36.1		

Microstructure and XRD results of the typical alloys after annealed at 1000 °C for 55 days are shown in Figures 2 and 3, respectively. Figure 2a–c shows the microstructure of the three-phase region of the alloys. In Figure 2a, the three-phase equilibrium of σ′ (black) + Ni_3Ta (gray) + C14 (light gray) in the $Ni_{59}V_{24}Ta_{17}$ alloy was established. Figure 2b shows the microstructure of the $Ni_{61}V_{30}Ta_9$ alloy, in which the black phase σ′, the white phase Ni_3Ta and the gray matrix fcc were observed. As displayed in Figure 2c, three-phase region of $NiTa_2$ + Ni_6Ta_7 + bcc-(Ta) in the $Ni_{19}V_{11}Ta_{70}$ alloy was identified. The light gray phase $NiTa_2$ precipitated in the matrix Ni_6Ta_7, along with the white phase bcc-(Ta). Figure 2d–f presents the microstructure of the two-phase section of the alloys. Figure 2d shows the two-phase section of bcc-(Ta) (gray) + C15 (black) in the $Ni_5V_{49}Ta_{46}$ alloy and the corresponding XRD result is shown in Figure 3a. Figure 2e is the microstructure of Ni_6Ta_7 (gray) + C14 (black) in the $Ni_{33}V_{25}Ta_{42}$ alloy. In the $Ni_{13}V_{46}Ta_{41}$ alloy annealed at 1000 °C for 55 days, two-phase equilibrium of C14 + bcc-(Ta) was confirmed in Figure 2f. The corresponding crystal structure was identified by XRD pattern in Figure 3b. In order to better identify the crystal structure of the C14 phase, we obtained single-phase alloys and the XRD result is presented in Figure 3c.

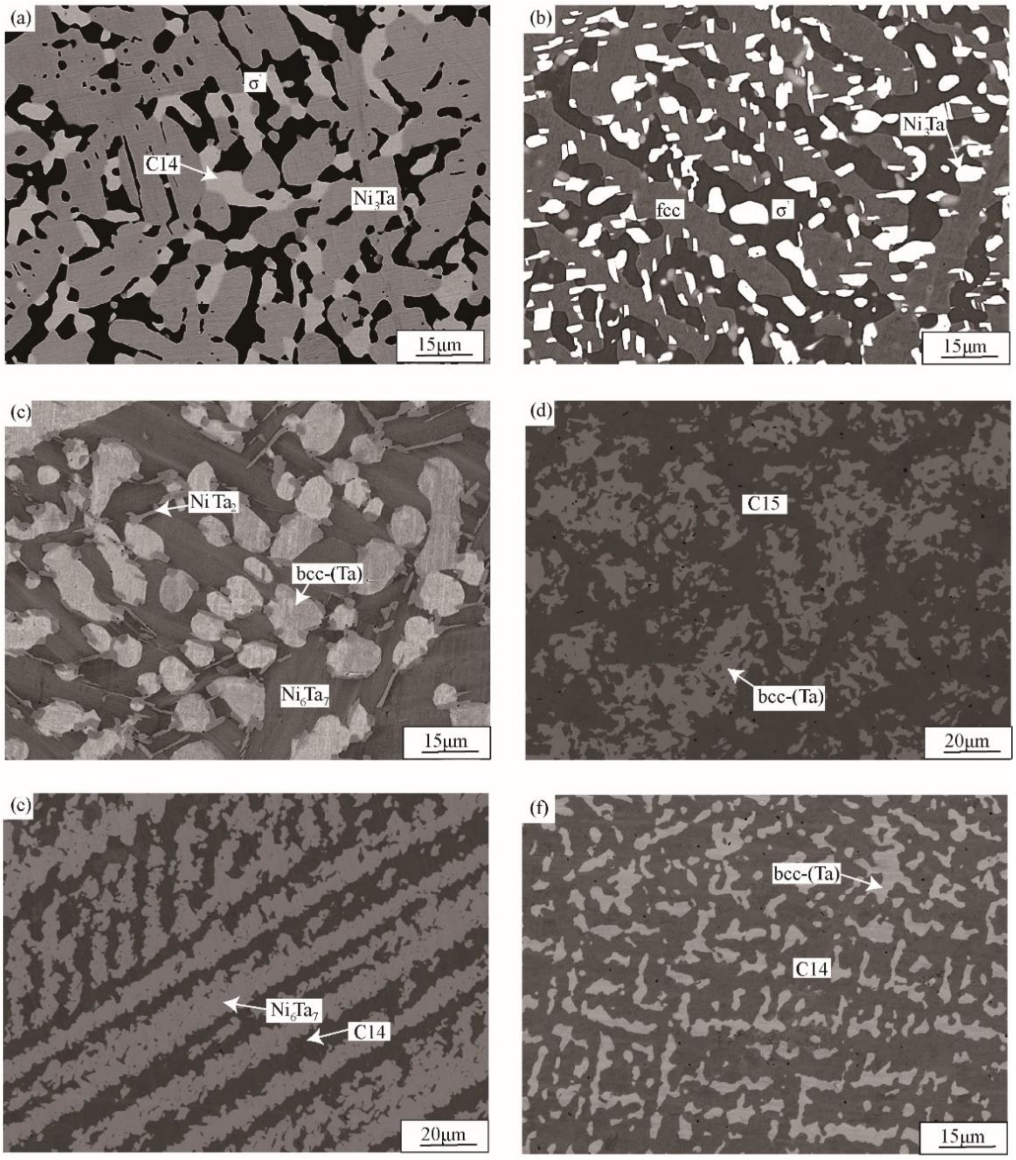

Figure 2. Microstructure of the typical alloys in the Ni-V-Ta system annealed at 1000 °C for 55 days. (**a**) $Ni_{59}V_{24}Ta_{17}$; (**b**) $Ni_{61}V_{30}Ta_{9}$; (**c**) $Ni_{19}V_{11}Ta_{70}$; (**d**) $Ni_{5}V_{49}Ta_{46}$; (**e**) $Ni_{33}V_{25}Ta_{42}$; (**f**) $Ni_{13}V_{46}Ta_{41}$.

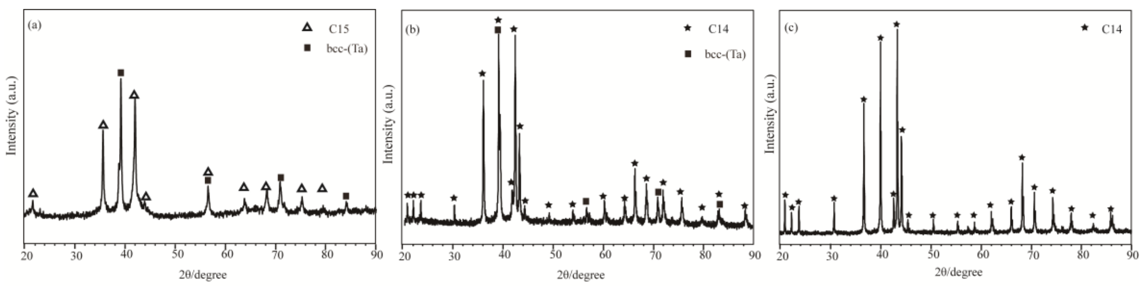

Figure 3. The XRD patterns of typical alloys in the Ni-V-Ta system annealed at 1000 °C for 55 days. (**a**) $Ni_{5}V_{49}Ta_{46}$; (**b**) $Ni_{13}V_{46}Ta_{41}$; (**c**) $Ni_{34}V_{33}Ta_{33}$.

According to the microstructure and XRD results, the isothermal section of the Ni-V-Ta system at 1000 °C is shown in Figure 4. Eight three-phase sections, σ′ + bcc-(V) + C14, fcc + σ′ + Ni_3Ta, C14 + σ′ + Ni_3Ta, fcc + Ni_3Ta + Ni_3V, C14 + Ni_6Ta_7 + Ni_3Ta, Ni_2Ta + Ni_6Ta_7 + Ni_3Ta, $NiTa_2$ + Ni_6Ta_7 + bcc-(Ta), and C14 + Ni_6Ta_7 + bcc-(Ta), were confirmed and marked by triangle with solid lines. Unfortunately, four three-phase equilibriums, fcc + Ni_8Ta + Ni_3Ta, fcc + Ni_3Ta + Ni_3V, C14 + C15 + bcc-(Ta) and C14 + C15 + bcc-(V) were not established and marked by triangle with dash lines. The determined two-phase region was marked in black fine lines and single phase with small squares. The experimental data indicate that: (1) a single-phase region C14 with a large solubility of three elements, which was measured to be 23.3–52 at. % V, 22.4–38.1 at. % Ta and 13.1–49 at. % Ni, exists at 1000 °C; (2) although the C14 phase is not found in V-Ta binary system at 1000 °C, it is stabilized by addition of Ni confirmed by the presence of a single-phase C14; (3) the Ni_3V phase was confirmed at 1000 °C near the Ni-V side, which did not form a continuous solid solution with the Ni_3Ta phase; (4) the phases fcc, Ni_3V and σ′ dissolve up to 5.8 at. %, 7.1 at. % and 5.9 at. % Ta, respectively; (5) the solubility of V in the phases Ni_3Ta, Ni_2Ta and Ni_6Ta_7 was determined to be 17 at. %, 3.8 at. % and 31.9 at. %, respectively.

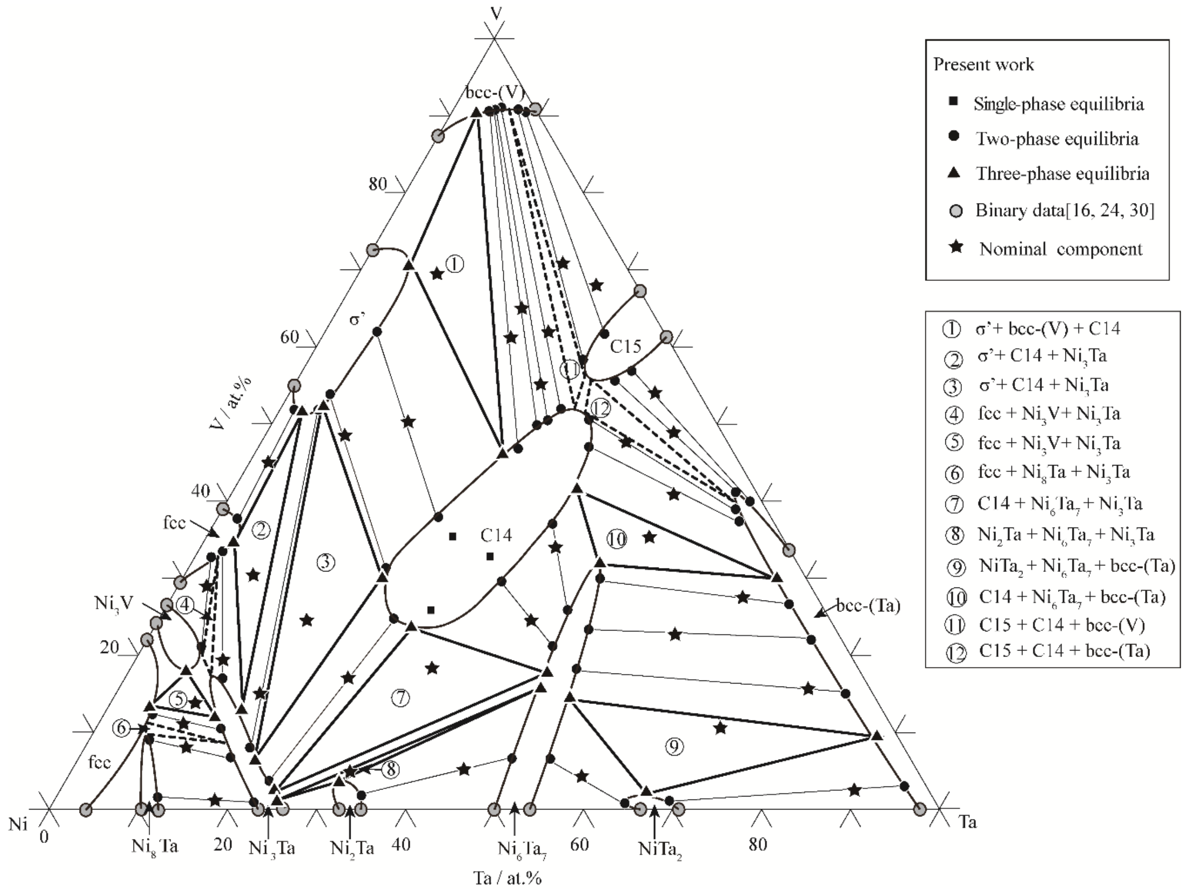

Figure 4. Experimentally determined isothermal section of the Ni-V-Ta system at 1000 °C.

3.2. Phase Equilibria at 1200 °C

Based on the experimental results, eight intermetallic compounds (σ′, Ni_8Ta, Ni_3Ta, Ni_2Ta, Ni_6Ta_7, $NiTa_2$, C14, C15) and two solid solutions—fcc and bcc—were confirmed at 1200 °C, as shown in Table 1. The isothermal section of the Ni-V-Ta ternary system at 1200 °C was established by 38 alloys summarized in Table 3.

Table 3. Equilibrium compositions of the phase in the Ni-V-Ta ternary alloys annealed at 1200 °C for 40 days except the starred ones.

Alloys (at. %)	Phase Equilibrium	Composition (at. %)					
	Phase 1/Phase 2/Phase 3	Phase 1		Phase 2		Phase 3	
		V	Ta	V	Ta	V	Ta
$Ni_{24}V_{67}Ta_9$	bcc-(V)/σ′/C14	85.1	4.1	66.2	6.5	43.6	24.6
$Ni_{13}V_{65}Ta_{22}$	bcc-(V)/C14	88.8	7.5	49.5	29		
$Ni_{41}V_{49}Ta_{10}$ *	σ′/L/C14	55.6	5.5	42.2	11.1	34.5	22.2
$Ni_9V_{41}Ta_{50}$	bcc-(Ta)/C14	33.2	66.4	45.6	37.3		
$Ni_{61}V_{30}Ta_9$ *	fcc/Ni_3Ta/L	34.2	4	9.1	27.5	37.3	11.8
$Ni_{75}V_{18}Ta_7$	fcc/Ni_3Ta	20.9	6.5	16.8	9.1		
$Ni_{59}V_{24}Ta_{17}$ *	Ni_3Ta/L/C14	6.4	20.2	37.5	12.2	26.3	23.7
$Ni_{48}V_{18}Ta_{34}$	Ni_3Ta/Ni_6Ta_7/C14	2.3	23.1	18.6	46	21	28.6
$Ni_{77}V_{14}Ta_9$	fcc/Ni_3Ta	15.1	6.2	10.8	14.1		
$Ni_{19}V_{11}Ta_{70}$	bcc-(Ta)/Ni_6Ta_7/$NiTa_2$	9.3	89.1	12.5	52.7	0.9	66.1
$Ni_{17}V_{61}Ta_{22}$	bcc-(V)/C14	88.3	6.6	48.3	28.1		
$Ni_{52}V_{45}Ta_3$ *	fcc/σ′/L	41.6	2	53.8	3	45.9	5
$Ni_{26}V_{34}Ta_{40}$	Ni_6Ta_7/C14	28.3	44.9	38	36.8		
$Ni_{68}V_{15}Ta_{17}$ *	Ni_3Ta/L	7.9	18.7	37.3	12		
$Ni_{64}V_5Ta_{31}$	Ni_2Ta/Ni_3Ta/Ni_6Ta_7	3.8	29.9	1.7	24.5	16	46.5
$Ni_{82}V_7Ta_{11}$	Ni_8Ta/Ni_3Ta	8	7.9	5.5	18.2		
$Ni_{18}V_{23}Ta_{59}$	Ni_6Ta_7/bcc-(Ta)	23.8	50	20.9	78.9		
$Ni_8V_{28}Ta_{64}$	Ni_6Ta_7/bcc-(Ta)	31.5	47.5	24.8	75		
$Ni_5V_{49}Ta_{46}$	C14/bcc-(Ta)	55	36.2	44.3	55.6		
$Ni_6V_{71}Ta_{23}$	C14/bcc-(V)	56.5	30.6	89.8	9.5		
$Ni_{35}V_{50}Ta_{15}$	σ′/C14	60.5	7.2	39.4	23.1		
$Ni_{71}V_{19}Ta_{10}$	fcc/Ni_3Ta	26.8	5.1	14.7	12.1		
$Ni_{79}V_{10}Ta_{11}$	fcc/Ni_3Ta	10.8	7.5	6.6	17.2		
$Ni_{50}V_6Ta_{44}$	Ni_2Ta/Ni_6Ta_7	2.1	32.5	8.1	48.5		
$Ni_{39}V_4Ta_{57}$	$NiTa_2$/Ni_6Ta_7	0.6	64.8	5.7	53.5		
$Ni_9V_2Ta_{89}$	$NiTa_2$/bcc-(Ta)	0.6	66.9	2.6	97.1		
$Ni_7V_{13}Ta_{80}$	Ni_6Ta_7/bcc-(Ta)	18	51.5	12.4	87.5		
$Ni_{59}V_{17}Ta_{24}$	Ni_3Ta/C14	4.7	21.5	24.4	25.1		
$Ni_{37}V_{35}Ta_{28}$	C14	35	28				
$Ni_{34}V_{33}Ta_{33}$	C14	33	33				
$Ni_{44}V_{26}Ta_{30}$	C14	26	30				
$Ni_3V_{57}Ta_{40}$	C14/C15	47	35.9	46.8	42.1		
$Ni_{13}V_{46}Ta_{41}$	C14/bcc-(Ta)	48.8	36.8	41.5	58		
$Ni_{14}V_{36}Ta_{50}$	Ni_6Ta_7/C14/bcc-(Ta)	34	44.5	40.9	37	30.1	68.8
$Ni_{18}V_{55}Ta_{27}$	C14/bcc-(V)	49.6	30.5	89.1	8.2		
$Ni_{81}V_1Ta_{18}$	Ni_8Ta/Ni_3Ta	1.5	12.1	0.9	22.1		
$Ni_{12}V_{62}Ta_{26}$	C14/bcc-(V)	54.1	30.4	89.3	9.1		
$Ni_{33}V_{25}Ta_{42}$	Ni_6Ta_7/C14	22.5	45	30.2	34.7		

* The alloys indicated with (*) were annealed at 1200 °C for 3 h.

The microstructure and the corresponding XRD analysis are presented in the Figures 5a–f and 6a–c, respectively. Figure 5a shows the three-phase equilibrium of C14 + σ′ + bcc-(V) in the $Ni_{24}V_{67}Ta_9$ alloy annealed at 1200 °C for 40 days. Figure 5b features the microstructure of the $Ni_{48}V_{18}Ta_{34}$ alloy. The small black phase Ni_3Ta and the white phase Ni_6Ta_7 were evenly distributed in the gray matrix phase C14. The corresponding phase relationship was identified by XRD result, in which the characteristic peaks of the C14, Ni_3Ta and Ni_6Ta_7 phases were labelled by different symbols, as presented in Figure 6a. In the $Ni_{14}V_{36}Ta_{50}$ alloy quenched from 1200 °C, the three-phase region of C14 (dark gray) + Ni_6Ta_7 (light gray) + bcc-(Ta) (white) was confirmed in Figure 5c and the corresponding XRD pattern is displayed in Figure 6b. Figure 5d features the microstructure of the $Ni_{19}V_{11}Ta_{70}$ alloy. The small light gray phase $NiTa_2$ and white block phase bcc-(Ta), along with the dark gray matrix phase Ni_6Ta_7 were discovered. As presented in Figure 5e, a three-phase section of

Ni_2Ta (light gray) + Ni_6Ta_7 (white) + Ni_3Ta (black) was identified in the $Ni_{64}V_5Ta_{31}$ alloy annealed at 1200 °C for 40 days, and its XRD result is shown in Figure 6c. Figure 5f is the microstructure of three-phase region of fcc + Ni_3Ta + L in the $Ni_{61}V_{30}Ta_9$ alloy annealed at 1200 °C for 3 h.

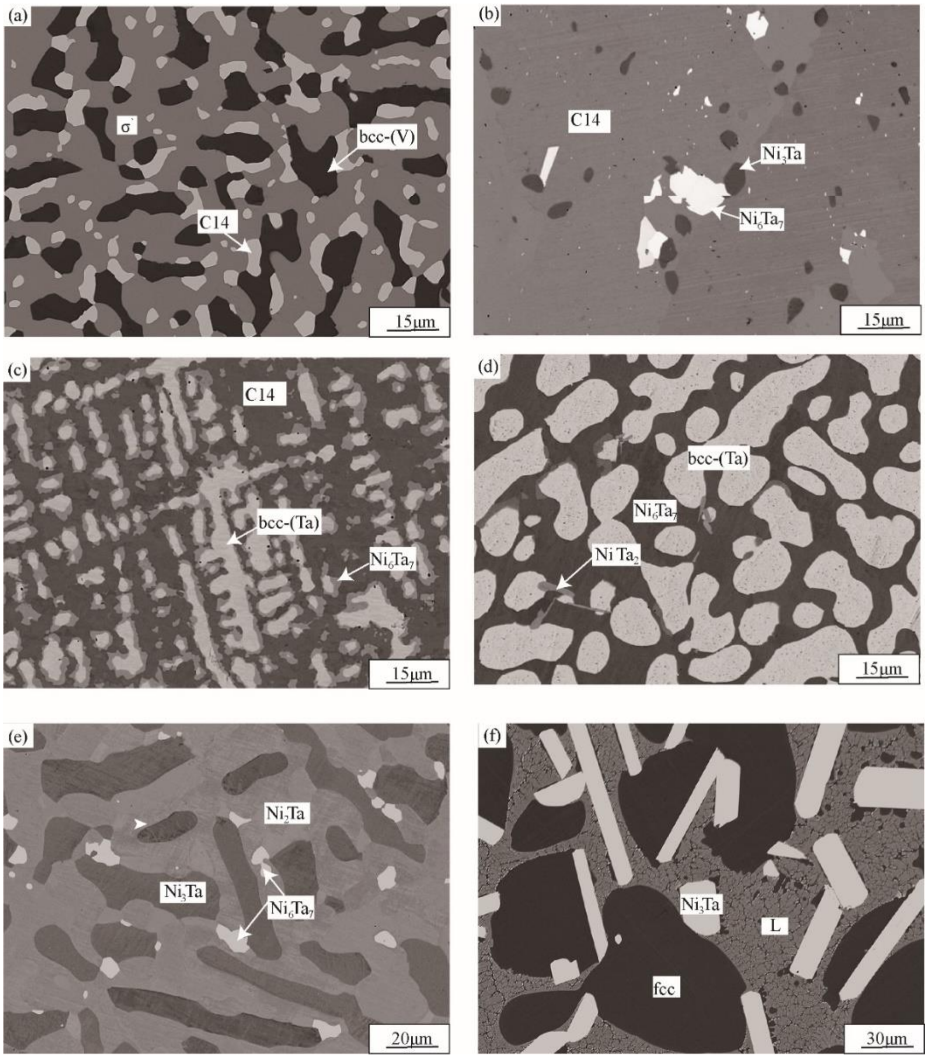

Figure 5. Microstructure of the typical alloys in the Ni-V-Ta system annealed at 1200 °C for 40 days. (**a**) $Ni_{24}V_{67}Ta_9$; (**b**) $Ni_{48}V_{18}Ta_{34}$; (**c**) $Ni_{14}V_{36}Ta_{50}$; (**d**) $Ni_{19}V_{11}Ta_{70}$; (**e**) $Ni_{64}V_5Ta_{31}$; and (**f**) the $Ni_{61}V_{30}Ta_9$ alloy annealed at 1200 °C for 3 h.

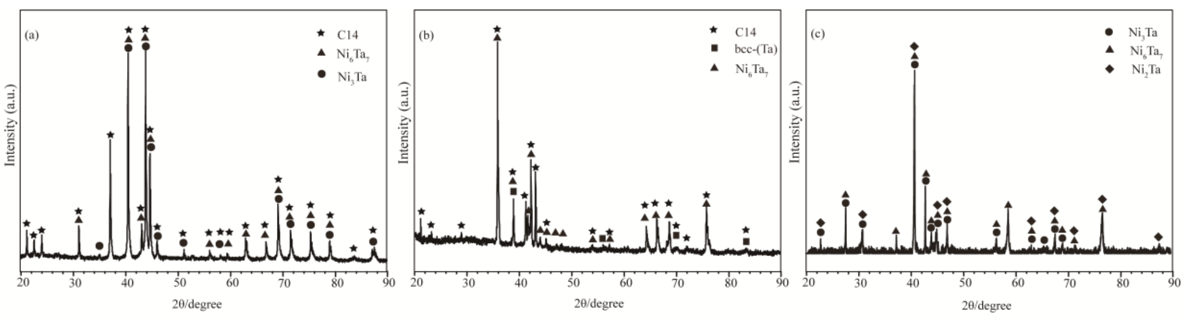

Figure 6. The X-ray diffraction (XRD) patterns of typical alloys in the Ni-V-Ta system annealed at 1200 °C for 40 days. (**a**) $Ni_{48}V_{18}Ta_{34}$; (**b**) $Ni_{14}V_{36}Ta_{50}$; (**c**) $Ni_{64}V_5Ta_{31}$.

Based on the experimental data mentioned above, the isothermal section of the Ni-V-Ta system at 1200 °C was established, as shown in Figure 7. Nine three-phase sections, σ′ + bcc-(V) + C14, σ′ + C14 + L, σ′ + fcc + L, fcc + L + Ni_3Ta, C14 + L + Ni_3Ta, C14 + Ni_6Ta_7 + Ni_3Ta, Ni_2Ta + Ni_6Ta_7 + Ni_3Ta, $NiTa_2$ + Ni_6Ta_7 + bcc-(Ta) and C14 + Ni_6Ta_7 + bcc-(Ta), were experimentally determined and presented as a triangle with solid lines. The other two three-phase equilibriums C15 + C14 + bcc-(Ta) and fcc + Ni_3Ta + Ni_8Ta were not confirmed and were displayed as a triangle with dashed lines. The corresponding results indicate that: (1) the C14 phase extends from the V-Ta side to the center and dissolves more Ni at 1200 °C, while the solubility of Ni in the C15 phase decreases than that at 1000 °C; (2) due to the congruent transformation fcc ↔ Ni_3V at 1045 °C, the Ni_3V phase disappeared at 1200 °C; (3) a small liquid region was detected; (4) the solubility of V in the phases Ni_3Ta, Ni_2Ta and Ni_6Ta_7 was measured to be around 17.2 at. %, 3.9 at. % and 33.8 at. %, respectively, which increases slightly as the temperature increases from 1000 to 1200 °C; (5) the phases fcc, σ′ and bcc-(V) dissolve about 6.2 at. %, 7.3 at. % and 10.1 at. % Ta, respectively.

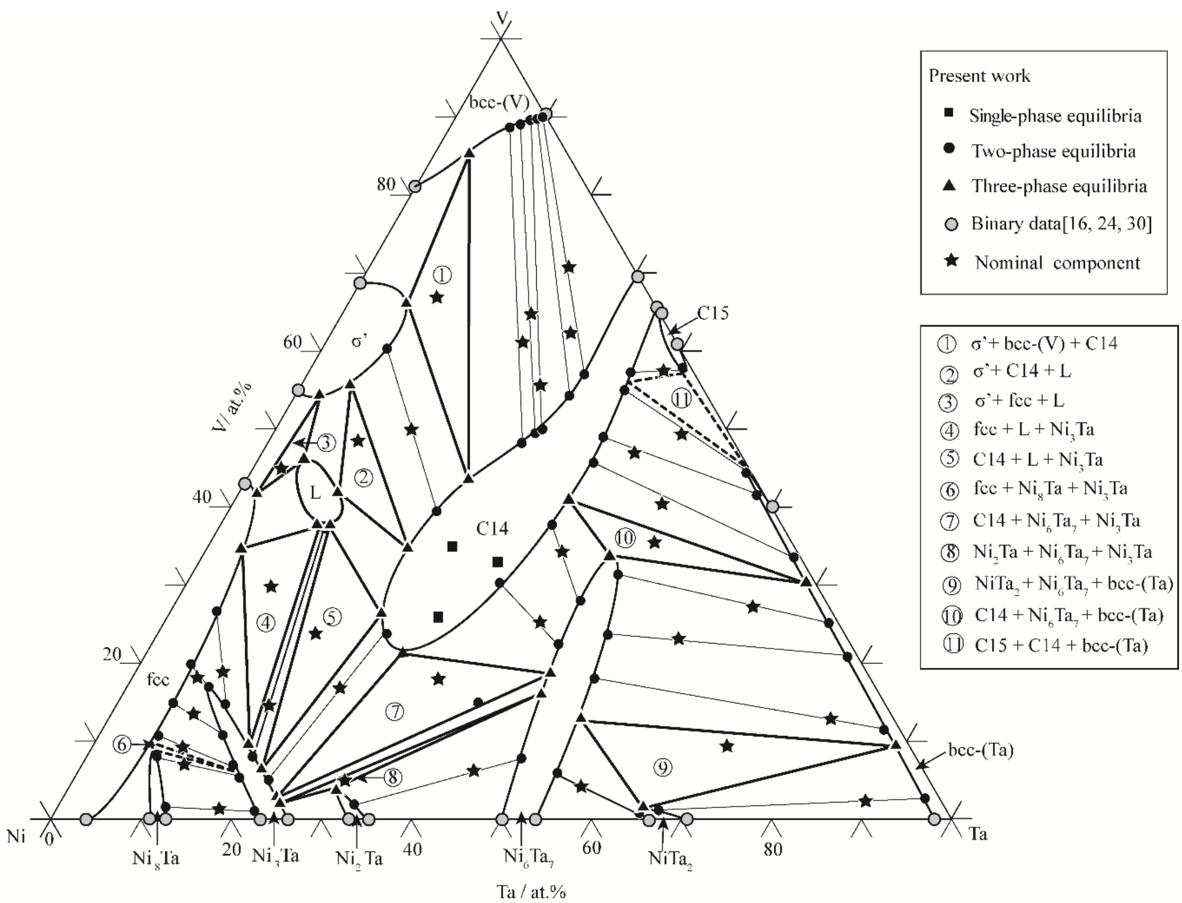

Figure 7. Experimentally determined isothermal section of the Ni-V-Ta system at 1200 °C.

3.3. Liquid Region

It is noticeable that a small liquid section was confirmed near the Ni-V side. As shown in Figure 2f, the bar-shaped white phase Ni_3Ta and the black phase fcc uniformly distribute in the liquid matrix. According to the eutectic reaction, L ↔ fcc + σ′ at 1202 °C in the Ni-V binary system, the eutectic microstructure is suggested to be consistent with the fcc and σ′ phase. In order to identify the temperature of phase transition, we conducted DSC analysis. With the DSC result shown in Figure 8, we observed that the σ′ phase transformed to the liquid phase when the temperature increased from 1100 to 1200 °C in the $Ni_{59}V_{24}Ta_{17}$ alloy. The melting point of the σ′ phase in the alloy was confirmed to be about 1137 °C. The corresponding results indicate that a third element addition of Ta in Ni-V alloys reduces the melting point of the alloys.

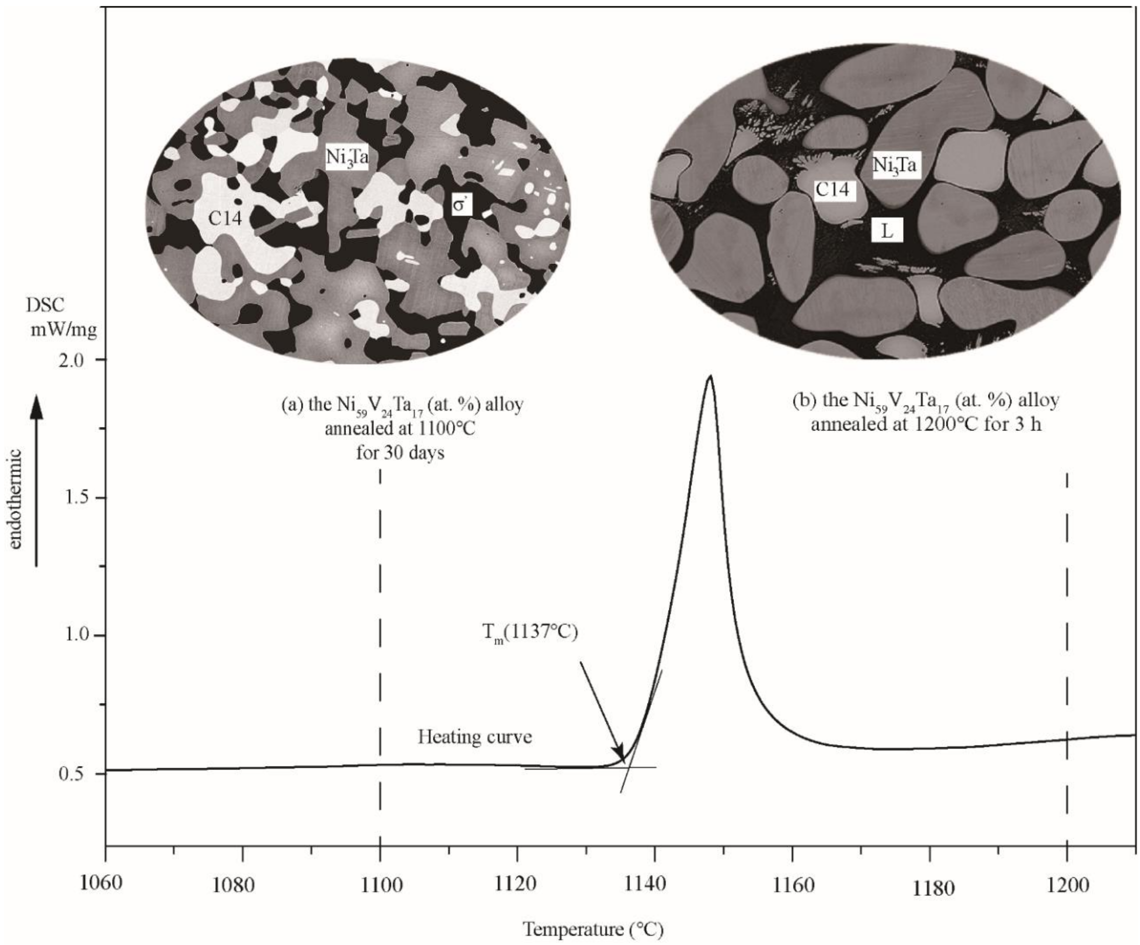

Figure 8. Heating curve of the $Ni_{59}V_{24}Ta_{17}$ alloy. The microstructure of the $Ni_{59}V_{24}Ta_{17}$ alloy annealed at (**a**) 1100 °C for 30 days; (**b**) 1200 °C for 3 h.

4. Conclusions

The results are shown as follows: (1) two isothermal sections of the Ni-V-Ta ternary system at 1000 °C and 1200 °C were experimentally established by the means of equilibrated alloy method; (2) the C15 phase dissolves less Ni, while the solubility of Ni in the C14 phase increases when the temperature raises from 1000 to 1200 °C; (3) the C14 phase was stabilized by addition of Ni against low temperature confirmed by the presence of a single-phase region at 1000 °C; (4) a small liquid phase was determined, while the Ni_3V phase just disappeared at 1200 °C; (5) the solubility of Ta in the phases fcc and σ′ increases as the temperature increases from 1000 to 1200 °C, while the solubility of Ni in the bcc-(Ta) phase shows the opposite tend. This research is of great significance to support the thermodynamic assessment of the Ni-V-Ta system.

Author Contributions: Conceptualization, C.W. and X.L.; Investigation, Y.L. (Yuhui Liang), Y.H. and J.Z.; Writing—Original Draft Preparation, Y.L. (Yuhui Liang); Writing—Review and Editing, S.Y., J.H. and Y.L. (Yong Lu) Supervision, X.L. and C.W.; Funding Acquisition, X.L. and C.W.

Funding: This research was founded by the National Natural Science Foundation of China (Grant No. 51831007).

Conflicts of Interest: The authors declare no conflict of interest.

References

1. Pollock, T.M.; Tin, S. Nickel-based superalloys for advanced turbine engines: Chemistry, Microstructure and Properties. *J. Propul. Power* **2006**, *22*, 361–374. [CrossRef]
2. Zheng, L.; Zhang, G.; Lee, T.L.; Gorley, M.J.; Wang, Y.; Xiao, C.; Li, Z. The effects of Ta on the stress rupture properties and microstructural stability of a novel Ni-base superalloy for land-based high temperature applications. *Mater. Des.* **2014**, *61*, 61–69. [CrossRef]
3. Huang, Y.; Mao, Z.; Noebe, R.D.; Seidman, D.N. The effects of refractory elements on Ni-excesses and Ni-depletions at γ(f.c.c.)/γ'(L12) interfaces in model Ni-based superalloys: Atom-probe tomographic experiments and first-principles calculations. *Acta Mater.* **2016**, *121*, 288–298. [CrossRef]
4. Yang, S.W. Effect of Ti and Ta on the oxidation of a complex superalloy. *Oxida. Met.* **1981**, *15*, 375–397. [CrossRef]
5. Park, S.J.; Seo, S.M.; Yoo, Y.S.; Jeong, H.W.; Jang, H. Effects of Al and Ta on the high temperature oxidation of Ni-based superalloys. *Corros. Sci.* **2015**, *90*, 305–312. [CrossRef]
6. Shibuya, S.; Kaneno, Y.; Yoshida, M.; Takasugi, T. Dual multi-phase intermetallic alloys composed of geometrically close packed Ni3X (X: Al, Ti and V) type structures—II. Mechanical properties. *Acta Mater.* **2006**, *54*, 861–870. [CrossRef]
7. Soga, W.; Kaneno, Y.; Yoshida, M.; Takasugi, T. Microstructure and mechanical property in dual two-phase intermetallic alloys composed of geometrically close-packed Ni3X (X: Al and V) containing Nb. *Mater. Sci. Eng. A* **2008**, *473*, 180–188. [CrossRef]
8. Kawahara, K.; Kaneno, Y.; Kakitsuji, A.; Takasugi, T. Microstructural factors affecting hardness property of dual two-phase intermetallic alloys based on Ni3Al-Ni3V pseudo-binary alloy system. *Intermetallics* **2009**, *17*, 938–944. [CrossRef]
9. Moreen, H.A.; Taggart, R.; Polonis, D.H. Ni8X phases in the systems Ni-V, Ni-V-Nb, and Ni-V-Ta. *J. Mater. Sci.* **1971**, *6*, 1425–1432. [CrossRef]
10. Gupta, K.L. The Ni-Ta-V (Nickel-Tantalum-Vanadium) System. In *Phase Diagrams of Ternary Nickel Alloys, Part 2*, 1st ed.; Indian Institute of Metals ASM International: Bidhannagar, India, 1990; pp. 208–213, ISBN 8185307113.
11. Kripyakevich, P.I.; Pylaeva, E.N. Crystal structure of the compound Ta_2Ni. *J. Struct. Chem.* **1962**, *3*, 35–37. [CrossRef]
12. Giessen, B.C.; Grant, N.J. The crystal structure of TaNi3 and its change on cold working. *Acta Metall.* **1967**, *15*, 871–877. [CrossRef]
13. Larson, J.M.; Taggart, R.; Polonis, D.H. Ni_8Ta in Nickel-rich Ni−Ta alloys. *Metall. Mater. Trans. B* **1970**, *1*, 485–489. [CrossRef]
14. Saburi, T.; Nakamura, M.; Nenno, S. Crystal structure and twin lamellae of Ni3Ta. *J. Less-Common Met.* **1975**, *41*, 135–139. [CrossRef]
15. Nash, P.; West, D.R.F. Ni–Al and Ni–Ta phase diagrams. *Met. Sci.* **1983**, *17*, 99–100. [CrossRef]
16. Nash, A.; Nash, P. The Ni–Ta system. *J. Phase Equilib.* **1984**, *5*, 444–445. [CrossRef]
17. Kaufman, L. Coupled thermochemical and phase diagram data for tantalum based binary alloys. *Calphad* **1991**, *15*, 243–259. [CrossRef]
18. Ansara, I.; Selleby, M. Thermodynamic analysis of the Ni-Ta system. *Calphad* **1994**, *18*, 99–107. [CrossRef]
19. Cui, Y.; Jin, Z. Experimental study and reassessment of the Ni-Ta binary system. *Z. Metallkd.* **1999**, *90*, 233–241.
20. Pan, X.; Jin, Z. Experimental determination and Re-optimization of Ni-Ta binary system. *Trans. Nonferrous Met. Soc. China* **2002**, *12*, 748–753. [CrossRef]
21. Zhou, S.H.; Wang, Y.; Chen, L.Q.; Liu, Z.K.; Napolitano, R.E. Solution-based thermodynamic modeling of the Ni-Ta and Ni-Mo-Ta systems using first-principle calculations. *Calphad* **2009**, *33*, 631–641. [CrossRef]
22. Zhou, Y.; Wen, B.; Ma, Y.; Melnik, R.; Liu, X. First-principles studies of Ni-Ta intermetallic compounds. *J. Solid State Chem.* **2012**, *187*, 211–218. [CrossRef]
23. Kosorukova, T.; Firstov, G.; Noel, H.; Ivanchenko, V. Crystal structure changes in the Ni3Ta intermetallic compound. *Chem. Met. Alloys* **2013**, *6*, 196–199.
24. Smith, J.F.; Carlson, O.N.; Nash, P.G. The Ni−V (Nickel-Vanadium) system. *J. Phase Equilib.* **1982**, *3*, 342–348. [CrossRef]
25. Stevens, E.R.; Carlson, O.N. V-Ni System. *Metall. Mater. Trans. B* **1970**, *1*, 1267–1271. [CrossRef]

26. Watson, A.; Hayes, F.H. Some experiences modelling the sigma phase in the Ni-V system. *J. Alloys Compd.* **2001**, *320*, 199–206. [CrossRef]
27. Kabanova, E.G.; Kuznetsov, V.N.; Zhmurko, G.P. Thermodynamic modeling of phase equilibria in the Ni-V system. *Russ. J. Phys. Chem. A* **2010**, *84*, 755–759. [CrossRef]
28. Savicky, E.M.; Efimov, J.V. Superconducting metallic compounds and their alloys. *Monatsh. Chem.* **1972**, *103*, 270–287. [CrossRef]
29. Smith, J.F.; Carlson, O.N. The Ta-V (Tantalum-Vanadium) system. *J. Phase Equilib.* **1983**, *4*, 284–289. [CrossRef]
30. Danon, C.A.; Servant, C. A thermodynamic evaluation of the Ta-V system. *J. Alloys Compd.* **2004**, *366*, 191–200. [CrossRef]
31. Okamoto, H. Ta-V (Tantalum-Vanadium). *J. Phase Equilib. Diffus.* **2005**, *26*, 298–299. [CrossRef]
32. Pavlů, J.; Vřešt'ál, J.; Chen, X.Q.; Rogl, P. Thermodynamic modeling of Laves phases in the Ta-V system: Reassessment using first-principles results. *Calphad* **2011**, *35*, 103–108. [CrossRef]